



HAL
open science

Quantitative evaluation of contactless impact echo for non-destructive assessment of void detection within tendon ducts

Franck Schoefs, Odile Abraham, John Popovics

► **To cite this version:**

Franck Schoefs, Odile Abraham, John Popovics. Quantitative evaluation of contactless impact echo for non-destructive assessment of void detection within tendon ducts. *Construction and Building Materials*, 2012, 37 (2012), pp.885-892. 10.1016/j.conbuildmat.2012.02.002 . hal-01007228

HAL Id: hal-01007228

<https://hal.science/hal-01007228>

Submitted on 16 Jun 2014

HAL is a multi-disciplinary open access archive for the deposit and dissemination of scientific research documents, whether they are published or not. The documents may come from teaching and research institutions in France or abroad, or from public or private research centers.

L'archive ouverte pluridisciplinaire **HAL**, est destinée au dépôt et à la diffusion de documents scientifiques de niveau recherche, publiés ou non, émanant des établissements d'enseignement et de recherche français ou étrangers, des laboratoires publics ou privés.



Distributed under a Creative Commons Attribution 4.0 International License

Quantitative evaluation of contactless impact echo for non-destructive assessment of void detection within tendon ducts

Franck Schoefs^a, Odile Abraham^b, John S. Popovics^c

^aLUNAM Université, Université de Nantes-Ecole Centrale Nantes, GeM, Institute for Research in Civil and Mechanical Engineering, CNRS UMR 6183, 2, rue de la Houssinière, BP92208, 44322 Nantes Cedex 3, France

^bLUNAM Université, IFSTTAR, MACS, CS4, 44344 Bouguenais Cedex, France

^c2129d Newmark Civil Engineering Laboratory, University of Illinois at Urbana – Champaign, 205 N. Mathews Ave., Urbana, IL 61801, USA

Owners of pre-stressed concrete structures must realize preventive maintenance in order to maintain structural safety and limit economic losses. Detection voids in tendon ducts, where corrosion could occur, is key in this effort. This paper focuses on the quantification of the performance of the impact echo method (IEM), applied using a new laser interferometer contactless robot, for duct void detection in a reinforced concrete wall. We show first the influence of the wall stiffness on the IEM (resonance) frequency. We use a probabilistic modeling to evaluate the IEM. We illustrate a way for accounting on-site uncertainties of NDT measurements.

Keywords:
Impact echo
Laser interferometer
Robot
Voids in tendon duct
POD PFA
ROC curve
 α - δ Method

1. Introduction

Preventive replacement of engineering structures results in high economic and environmental costs. Thus much effort is placed on maintaining these structures with efficient management plans. The challenge for the owners consists of guaranteeing the operation and safety of aging structures while ensuring reasonable costs and operational availability. Pre-stressed and post-tensioned concrete structures are especially important in this regard since the potential internal defects (void in the grout fill material within ducts) are critical to the safe performance of the structure but are difficult to detect. As such, owners base their maintenance decision schemes mainly on structural integrity assessment and consequence analysis. The major inputs come from information collected by inspections that employ non-destructive or destructive tools. The uncertainties and errors of these measurement can lead to bad decisions, but yet are rarely integrated into the decision process. Currently, Risk Based Inspection (RBI) [1–5], provides the basis for optimizing the maintenance plans of existing structures while ensuring satisfactory safety and operational availability of the structure throughout its service life. RBI depends both on reliability computations and probabilistic modeling of inspection results.

The condition assessment of the corrosion of tendons within the structure is critical. Currently, the condition of the tendons cannot be reliably assessed without excavating the duct to determine the presence of voids within tendon duct fill material, where tendon corrosion could take place, or evidence of cable rupture. Gamma ray radiography has been shown to be efficient for detection of these problems, but it is costly, demands trained and licensed personnel, and poses safety risks.

Assessment of existing structures normally requires updated material properties with reliable techniques. Generally, on-site inspections are necessary and visual inspections alone are not sufficient. Non Destructive Testing (NDT) tools are helpful in this regard. When inspecting large structures (bridges) or coastal and marine structures, the natural environment (wind, waves) and human factors (access, tiredness, lack of inspector experience, etc.) induce inferior conditions for inspection in comparison to laboratory conditions. In this context, the cost of inspection can be prohibitive and an accurate description of the on-site performance of NDT tools must be provided. When inspection of existing structures is not carried out under ideal conditions, it has become a common practice to model inspection method reliability in terms of Probability of Detection (PoD), Probability of False Alarms (PFAs) and Receiver Operating Characteristic (ROC) curves [6,7]. These general concepts are applied here for the case of defect detection in reinforced concrete structures. These parameters are generally the main inputs needed by owners of structures who are looking

to achieve the so-called IMR (Inspection, Maintenance and Repair) plan through Risk Based Inspection (RBI) methods.

First, this paper reviews theoretical aspects of detection theory and probabilistic modeling of inspections results. Then the paper presents the experimental program carried out on a specific wall using impact echo data collected in a contactless fashion using a robot. Finally the results are evaluated in terms of PoD, PFA, void detection capability and detection threshold calibration. The principal aim of the paper is to illustrate the potential of probabilistic modeling; the procedure and data presented herein can be implemented in a generic way to other NDT methods and inspection problems.

2. Probabilistic modeling of inspection based on detection theory

2.1. Probability of detection and probability of false alarm

The most common approach to characterize the performance of inspection tools is PoD. Let a_d be the detection threshold, below which it is assumed that no detection is possible. PoD is defined as:

$$\text{PoD} = P(\hat{D} \geq a_d) \quad (1)$$

where $P()$ represents a probability measure, \hat{D} is a variable that represents the measured defect size \hat{d} (response level of NDT tool i.e. 'signal + noise'). The real defect size (i.e. the real signal without noise) is D . Note that a_d can be defined either by calibration tests or based on the experience of the inspector.

Assuming that we know the probability density functions of noise and signal amplitude, by fitting an empirical distribution for instance, PoD and PFA are obtained:

$$\text{PoD} = \int_{a_d}^{+\infty} f_{\hat{D}}(\hat{d}) \partial \hat{d} \quad (2)$$

$$\text{PFA} = \int_{a_d}^{+\infty} f_A(\eta) \partial \eta \quad (3)$$

where $f_{\hat{D}}$ and f_A are the probability density functions of the 'signal + noise' \hat{D} (or measured defect) and the 'noise' A , respectively. The integrations in Eqs. (2) and (3) are carried out across all measured defect sizes.

Thus, PoD is a function of the detection threshold, the measured defect size and the noise while PFA depends on the detection threshold and noise only [8]. Noise is dependent on the decision-chain "physical measurement-decision on defect measurement transfer of information" [8,9], the conditions of inspection (harsh environment, surface quality, electronic noise, etc.) and the complexity of testing procedure (accessibility, mounting of the device, etc.). In the following we show that it is better to define it base on the best compromise between the increase of PoD and the decrease of PFA.

Fig. 1 illustrates the Probability Density Function (PDF) and the area to be computed for the evaluation of PoD and PFA for a given detection threshold in the case where the PDFs for 'signal + noise' \hat{D} and 'noise' A are normally distributed.

2.2. Receiver Operating Characteristic (ROC) curve

The ROC curve links the Probability of Detection and the Probability of False Alarm. For a given detection threshold, the pair (PFA, PoD) defines NDT performance. This pair can be considered as coordinates of a point in R^2 (square integrable space of real numbers) with axes representing PFA and PoD. Let us consider that a_d takes values in the range $-\infty$ to $+\infty$. The resulting set of coordinates form points that belong to a curve called Receiver Operating

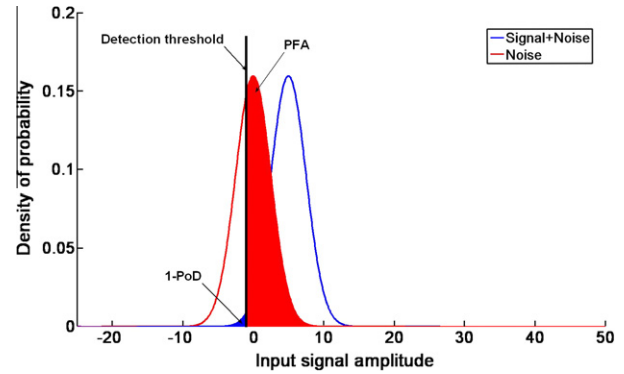


Fig. 1. Illustration of PoD and PFA (signal + noise with noise normally distributed) for a given detection threshold.

Characteristic (ROC), which is a parametric curve with parameter a_d and defined by Eq. (2) and (3) [6].

The example of the ROC curve (ROC 3) plotted on Fig. 2 is computed with the PDF presented on Fig. 1, assuming normal distributions.

The ROC curve is a fundamental characteristic of NDT tool performance for a given defect size. Perfect performance is represented by a ROC curve reduced to a single point whose coordinates are: (PFA, PoD) = [0, 1]. The ROC curve represents NDT tool performance facing a given PDF of a defect or a defect range. More details are available elsewhere [6].

Fig. 2 presents three theoretical ROC curves, each one corresponding to a different NDT tool performance. The worst curve is ROC 1, meaning that noise can be easily detected as a defect even if nothing is to be detected; this will lead to a high number of false alarms. As a result, overall performance will be poor. In contrast, the best performance is represented by ROC 3, which differs considerably with the previous curve. The probability of detection reaches values near 1, with small probabilities of false alarms for high values of PoD. Overall performance will be very good.

ROC curves can be obtained by considering two techniques and the same defect range, or one technique and two defect ranges, or one technique with two settings and the same defect range, or one technique applied under various conditions, even if the testing procedure is rigorously maintained during inspection. This latter case applies to underwater inspections of marine/coastal structures where accessibility and visibility are limited and conditions for the use of NDT tools are not optimal [8].

A simple geometric characterization of ROC curves is the minimum distance between the curve and the best performance point (BPP) at coordinates (PFA = 0, PoD = 1) [9]. By definition, the bigger

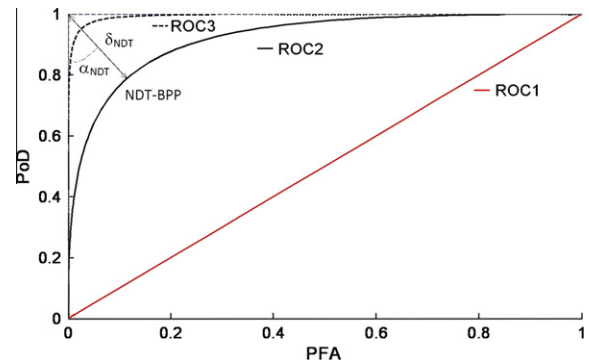


Fig. 2. Example of ROC curves with different levels of NDT performance from poor (ROC 1) to excellent (ROC 3).

the distance, the worse is the performance represented by the ROC curve. The point on the ROC curve corresponding to the minimum distance between BPP and the curve is called the performance point of the NDT tool (NDT-BPP). This distance (Euclidean measurement) can thus be considered as a measure of performance. But, a given measure can be obtained with several shapes of ROC curves, which is why this paper defines a curve characterization by using the polar coordinates of the NDT-BPP. The NDT-BPP polar coordinates are defined by (Fig. 2):

- the radius δ_{NDT} α_{NDT} equals the performance index (NDT-PI) (distance between the best performance point and the ROC curve) [8–10];
- the α_{NDT} δ_{NDT} is the angle between axis (PFA = 0) and the line (BPP, NDT-BPP).

It has been shown in [10] that α_{NDT} is essential to provide complete risk analysis, including consequence assessment after inspection. However, such a study is beyond the scope of this particular study so this parameter will not be analyzed here. Assessment of PoD and PFA from the knowledge of detection threshold can be directly deduced from calibration (measure knowing the defect) of NDT tools from statistical analysis of inspection results [11,12]. Generally these projects are expensive, and consequently it is sometimes necessary to choose another approach. Calculation of PFA and PoD thereby results from probabilistic modeling of the ‘noise’ and ‘signal + noise’ PDF [8,10].

2.3. Statistically based ROC computation

Here assume that the NDT tool is still under development and the detection threshold is unknown. This paper shows how to build ROC curves from statistics and then to deduce the best detection threshold in terms of α_{NDT} and δ_{NDT} . We compute PoD and PFA by [13]

$$\text{PoD} \approx \frac{\text{Card}(A)}{n_m} \quad \text{with} \quad A = \{i \in \mathfrak{I}; \hat{d}_i > a_d\} \quad (4)$$

$$\text{PFA} \approx \frac{\text{Card}(B)}{n_m} \quad \text{with} \quad B = \{i \in \mathfrak{I}; \eta_j > a_d\} \quad (5)$$

where $\text{Card}(\cdot)$ indicates the cardinal of a particular set and $\mathfrak{I} = \{1, \dots, n_m\}$. n_m denotes the number of measurements.

3. Testing procedure

3.1. Contactless impact echo measurements collected with a robot

Impact echo is a non-destructive resonance-based method that has been developed more than 20 years ago. Most often it is applied to concrete slabs to measure thickness or to detect defects such as voids or delaminations that are characterized by a change of mechanical impedance within the base material [13]. It is now clearly established for slab and wall structures that the impact echo thickness resonance phenomenon is associated with the Zero Group Velocity frequency of the first symmetric Lamb mode of the wall or plate structure [15,16]. It appears thus that the thickness resonance frequency is dependent on the local stiffness through the thickness of the wall. The wall thickness resonance frequency f_p is related to the compression wave velocity V_p of the wall material and to the wall thickness e by:

$$f_p = \beta \frac{V_p}{2e} \quad (6)$$

where β is a shape factor function that depends on the Poisson ratio ν [15]; its value for $\nu = 0.22$ is equal to 0.95 based on the established Lamb wave interpretation of the behavior [15,16].

Impact echo has also been applied as an NDT tool to detect grout filling voids within tendon ducts in concrete structures. When an impact-echo test is carried out on a thickness section that contains a void, the thickness resonance frequency is lowered notably and a secondary, high frequency resonance peak, usually named f_{void} , can appear [14]. The latter phenomenon is harder to observe in practice because of experimental limitations and is not considered herein. Here we investigate the modification of the thickness resonance frequency of a reinforced concrete wall that contains ducts of various filling conditions.

To carry out our measurements we have designed a robot that generates and records impact echo signals across the 1.5 m × 1.9 m surface of the concrete wall test sample. The source consists in an impact by a steel ball (here of diameter 16 mm) that is controlled by an electro magnet. The receiver is a laser interferometer from Polytec PI (OFV-505 sensor and OFV-5000 controller) with a VD-Q2 demodulator that has a sensitivity of 5 mm s⁻¹ V⁻¹ and a bandwidth from 0 to 250 kHz. The acquisition software has been designed to perform signal averaging (here three signal stacks for each test point are performed) and automatic auto-focus to ensure a good signal to noise ratio. For the experiment conducted here the signal acquisition frequency is 1.2 MHz and 4096 points are recorded. The Bakelite wood-form used during casting of the wall ensures a flat surface, and no additional surface preparation is needed to record the impact-echo signal with the laser interferometer.

3.2. Detail of the full scale wall and section of ducts

A reinforced concrete wall test sample was designed to illustrate the influence of the wall inner structure, including tendon ducts with varying fill condition, on impact echo signals. The wall is 0.25 m thick, 1.9 m high and 1.5 m wide. The concrete (CEM 1 52.5 N) has a 28-day compressive strength of 33 MPa. A photo of the wall before casting is shown in Fig. 3, and the concrete composition is given in Table 1. In the upper part of the wall some additional steel reinforcing bars were added to ease its carrying by a traveling crane; additional steel elements are also inserted in the lower part of the wall for the same purpose.

The wall is divided in two sections (Left and Right), each having each four horizontal tendon ducts. They are numbered 1–4 from top to bottom (Fig. 3). The duct sections are named with a letter L or R for Left or Right, and a number from 1 to 4 depending of their position. The distance between the ducts is 0.346 m (around eight

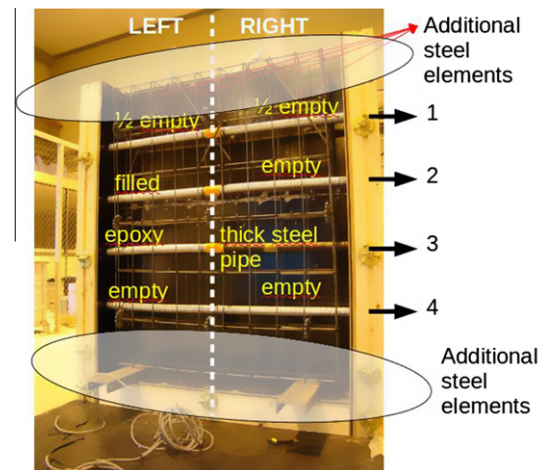


Fig. 3. Photo of the internal structure of the concrete wall showing the four lines of duct.

Table 1
Concrete composition (in kg per m³).

Sand 0/4 mm	810 kg
Granulates 2/10 mm	130 kg
Granulates 11.2/22.4 mm	870 kg
Cement (CEM 1 52.5 N)	334 kg
Chateaufuil (Mont-Gens sur Loire) filler	48 kg
Adjuvant viscoconcrete 3045	0.62 kg
Water	182.5 kg

times their diameter) so that it is possible to measure the wall thickness by impact echo measurements in between the ducts [17]. The left and right sections of one duct line are connected by tape.

Table 2 summarizes the information about each duct. All the tendon ducts except for duct R3 have a external diameter of 0.04 m and an internal diameter of 0.038 m and are made of steel strip sheaths. Duct R3 is a thick steel pipe (wall thickness 5 mm). Unless noted otherwise the grout that fills the duct is Superstresscem[®]. One tendon duct is filled with epoxy (L3) to represent filling with degraded mechanical characteristics. All the ducts contain, centered in their middle, one steel multi-wire cable, except for ducts L4, R4, and R3.

It is important to note that the wall itself does not have consistent properties from top to bottom. Indeed, as previously stated, the regions nearby and above the duct set 1 (topmost) and nearby and below the lower duct set 4 (bottommost) are more heavily reinforced with steel bars (Fig. 3). These regions are stiffer through the thickness section than the central region of the wall. We will refer to these areas as “highly reinforced concrete” whereas the space between the ducts will be denoted as “ordinary concrete”.

3.3. Testing procedure and selection of a quantity of interest

For each impact echo test, the impact point and the measurement point are positioned 0.015 m apart, aligned horizontally. The test point measurement grid has a horizontal spacing of 0.02 m and a vertical spacing of 0.03 m. The measurements are performed line by line and, at the end of each individual line, the robot comes back to a fixed position to test the consistency of the measurements.

Fig. 4 shows one individual impact-echo time signal and its Fourier transform. The frequency corresponding to the maximum amplitude is the thickness resonance frequency, f_p , and is hereafter considered as the parameter of interest from each test point of the grid. The resolution of the Fourier transform spectra is $df = 244$ Hz. Within the investigated zone, meaningful peak frequencies vary between 6 kHz to 9 kHz [two limit frequencies hereafter named $f_{p,low}$ and $f_{p,up}$]. Peak frequency outside the range $[f_{p,low}, f_{p,up}]$ can be linked to measurement perturbations such as surface disorder (typically air bubbles at the surface) that lead to poor signal detection with the laser interferometer. Signals that were deemed to be of insufficient quality were removed from the database and not considered in the analysis.

Table 2
Description of the tendon ducts embedded within the concrete wall test sample 1.

	Left	Right
1	1L: half empty (horizontal filling with Superstresscem [®])	1R: half empty (vertical filling with Superstresscem [®])
2	2L: fully filled with Superstresscem [®]	2R: empty
3	3L: filled with epoxy	3R: thick empty steel pipe/no cable
4	4L: empty/no cable	4R: empty/no cable

3.4. Signal modeling for ROC curve construction

In this paper the test parameter selected for void detection is the peak frequency f_p because it is linked to the wall section stiffness. This approach can obviously be extended to other test parameters of interest. Fig. 5 presents the impact echo peak frequency data from each test location on the wall, where solid lines indicate the location of the ducts. The presence of lower stiffness regions is associated with empty or partially empty ducts, or ducts filled with epoxy. The presence of high stiffness regions is associated with highly reinforced sections, for example at the top of the wall. We can associate the presence of a defect, i.e. a void, with a region of lower frequency. Thus, the peak frequency of the region outside the duct area is called here “noise”. When performing the test nearby a duct, the stiffness of the neighboring concrete represents the noise and the global measure is the “signal plus noise” $\hat{f}_{p,i}$ so Eqs. (4) and (5) become:

$$\text{PoD} \approx \frac{\text{Card}(A)}{n_m} \quad \text{with} \quad A = \{i \in \mathfrak{I}; \hat{f}_{p,i} < a_d\} \quad (7)$$

$$\text{PFA} \approx \frac{\text{Card}(B)}{n_m} \quad \text{with} \quad B = \{i \in \mathfrak{I}; \eta_j < a_d\} \quad (8)$$

Note that the inversion of the sign for the inequality in the definition of A and B , as compared with Eqs. (4) and (5), is due to the fact that PDF of ‘noise’ and ‘signal + noise’ are inverted: in Fig. 1, the noise PDF is on the left side and does not have a mean value of zero.

In the following, a complete risk and cost analysis, such as that reported in [10], is not performed; rather, we restrict this study to δ_{NDT} computation. Actually, α_{NDT} plays a role only if the effect of the shape of the ROC curve can be taken into account in a risk analysis by introducing consequences of the inspection result; this is beyond the scope of this paper.

4. Results and analysis

4.1. Pre-treatment of data

First, the original data must be pre-treated to remove non-physical measurements (due to the air bubble on the surface that perturb the laser interferometer). The flowchart in Fig. 6 shows two main steps:

- Step 1: pre-processing by filtering all the data outside the interval $[f_{p,low}; f_{p,up}]$;
- Step 2: pre-processing by removing data near the horizontal boundary between concrete and duct, at the lower part of the wall and at the end of the duct, and between two aligned ducts where a void in connection occurs. Measurements in this area are perturbed by wave scattered by the duct [17] and are not representative of a typical measurement above the duct or of a measurement far from a duct.

Due to the configuration of the wall, we distinguish two type is signal noise: one from the *ordinary concrete section* and the other from the *highly reinforced concrete section*.

Fig. 7 shows mean peak frequency data plotted along horizontal-axes across the ordinary concrete section, the highly reinforced concrete section, and the left and the right sections of duct 1. The data in Fig. 7 show that the peak frequencies of concrete and ducts can be easily distinguished. Moreover, the ends of the duct and the connections between ducts (indicated in the photo inset in this figure) show some disruption to the signal. This disruption effect is linked to the fact that the peak frequency is sensitive to the

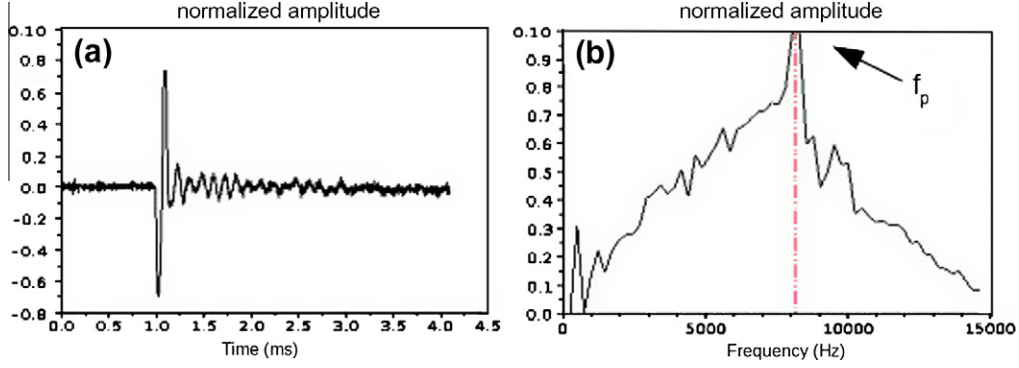


Fig. 4. (a) One impact echo normalized time signal and (b) the modulus of its Fourier transform (normalized).

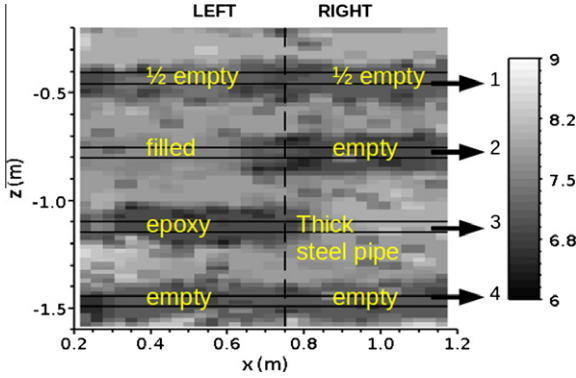


Fig. 5. Map of peak frequency at each test point across the wall area.

average stiffness around the measurement point, which is affected by edges and through thickness average stiffness.

4.2. Consistency tests

Before analyzing the capability to detect defects according to the ROC criteria, measurement consistency tests were carried out. After each line of horizontal measurement, the robot goes back to a reference point P_{ref} at the top-left of the wall before measuring the next line. This test checked for progressive deviation of measurements during the test and confirmed that the scatter between the mean measured value at P_{ref} and other measurements at the same point follows a classical symmetric single mode distribution [6,8]. The standard deviation of the data obtained from this repetitive test was reasonable (101 Hz) and the coefficient of variation only 1.5%. If we look to the measurements performed on concrete above and outside the duct area, the difference between mean values of peak frequency is about 3 kHz: this scatter covers stiffness variation of the concrete wall as well as the error of measurement and artifact coming from disruption caused by edge effects. It is clear that error of measurements does not affect void detection capability. Both error of measurement and local stiffness variations are referred to as “noise” in the following.

4.3. ROC construction and δ computation

From the statistical distribution of the measurements within each zone, we deduce the couple PoD and PFA couple at each detection threshold a_d by using Eqs. (7) and (8). We distinguish two types of noise: that from the ordinary concrete section and that from the highly reinforced concrete section. The highly reinforced concrete is localized at the top and bottom of the wall, and it differs from the

ordinary section because of the presence of additional steel reinforcing bars (Fig. 3). In the following, we present only two most representative cases to illustrate:

- Case 1: filled duct in ordinary concrete (3L); results shown in Fig. 8;
- Case 2: empty duct without tendon in highly reinforced concrete (4R); results shown in Fig. 9.

From these two cases, it appears that the discrepancy between frequencies of the “noise” and “signal + noise” is much lower in case 1 than in case 2 where two modes of the distribution (interval of maximum probability) can be clearly identified and distinguished.

Fig. 10 plots seven most pertinent ROC curves obtained along the ducts: the data from duct 2L were not included since it is not detectable with IEM tests; nevertheless data from duct 2L are used in the PoD and PFA assessments. The shape of the curves are different from each other, and one of them (duct 3R) forms part of NDT tool rejection in the (PFA; PoD) graph: PFA > PoD. In that case (thick-walled steel empty duct) the method has limited capability to detect a void in comparison to the surrounding thickness resonance frequency. This is due to the stiffness of the thick steel pipe itself. This result shows that the stiffness of the section, rather than the presence of a void, has the most effect on the impact echo resonance frequency. Void detection using impact echo should thus be carried out carefully considering information about inner reinforcement and the duct stiffness properties. Comparison of peak frequencies along the duct itself is preferred. In this context scanners, such as the one presented here or others [18], are useful as they produce 2-D maps. Table 3 gives the values obtained for δ_{NDT} for each of the 7 ROC curves, including ducts in highly reinforced concrete section. The precision of the δ_{NDT} measure is about 0.015. This distance δ_{NDT} varies from 0.125 to 0.867 (ordinary concrete section background) and appears to be very sensitive to the duct condition. The minimum values are obtained for ducts 1R, 2R, 4L, and 4R (0.025) and the maximum value occurs for duct 3R (0.593) with the highly reinforced concrete background. Note that the ranking of ducts according to δ_{NDT} is similar regardless of the concrete condition:

- For ordinary concrete sections: $3R > 1L > 3L > 1R \approx 2R \approx 4L \approx 4R$
- For highly reinforced concrete sections: $3R > 1L > 3L > 1R = 2R = 4L = 4R$

It appears that ducts that themselves have high nominal stiffness, such as the thick-walled steel duct in section 3R, do not lend themselves to inspection with impact-echo when the background data considered are the concrete outside the duct area. The

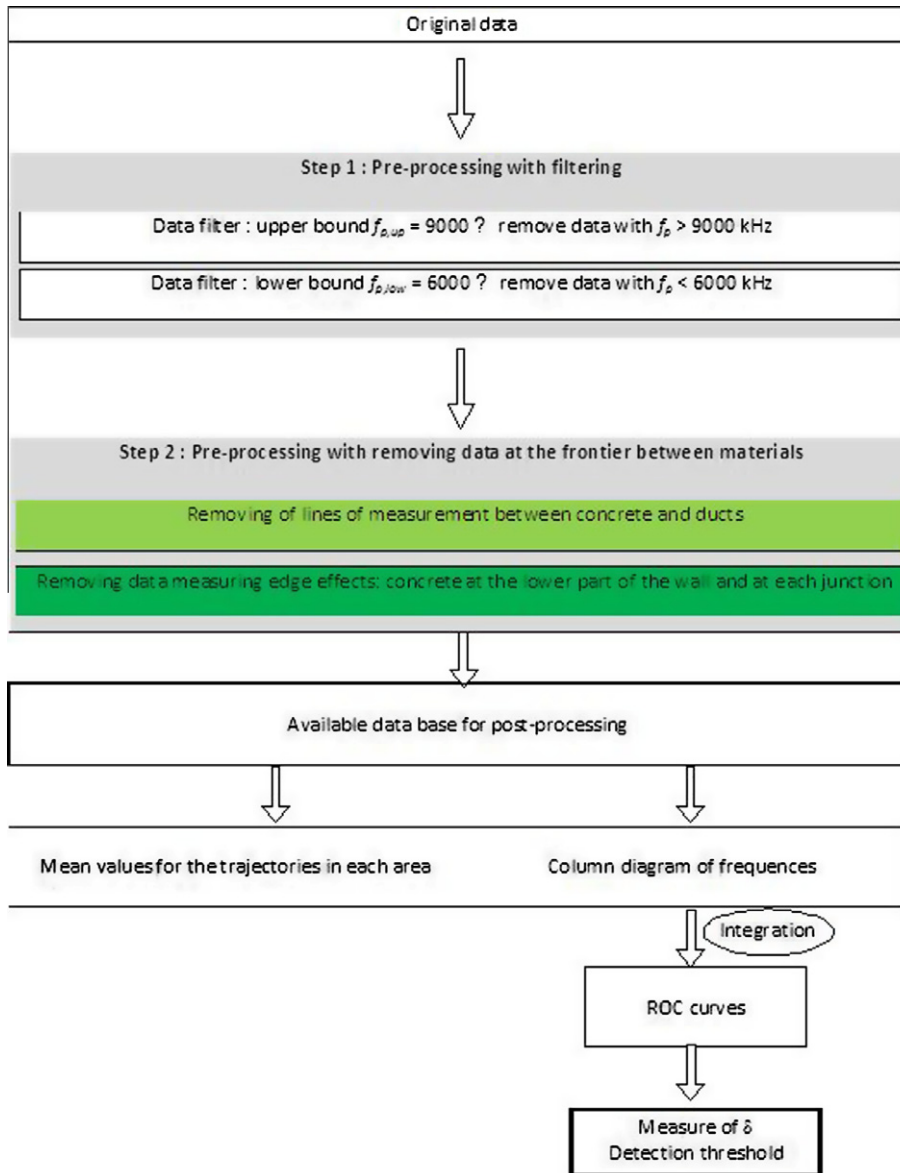


Fig. 6. Flowchart illustrating data pre- and post-processing processes.

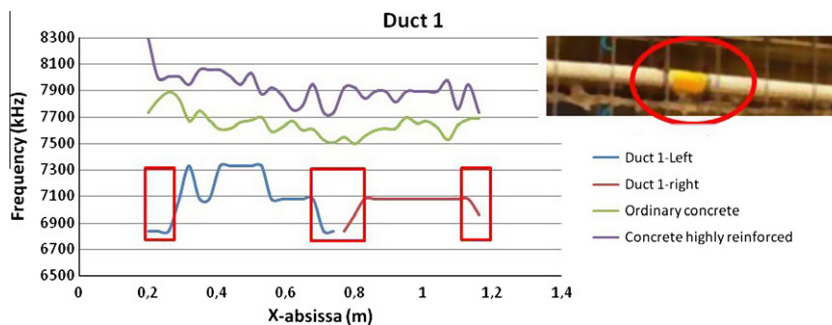


Fig. 7. Variation of mean of the peak frequencies along path of duct 1 and reference paths.

detection capability is more difficult for the duct half filled (void at the upper side) with superstresscem[®] grout (1L) and the duct filled with epoxy (3L). Finally, the detection of the void with an half vertical filling of the duct (1R), of an empty duct with (2R) or without tendon (4L, 4R) leads to the same detection capability

with this proposed protocol and they cannot be distinguish further.

Considering the relative detection ability in ordinary and highly reinforced sections of the test wall, the relative decrease of δ_{NDT} can be interpreted in terms of gain of detection capability. The

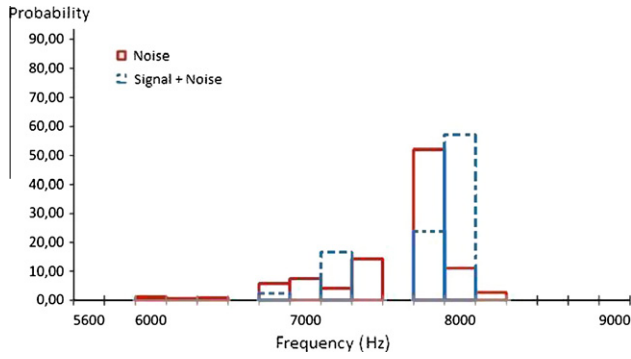


Fig. 8. Column diagrams for signal and signal + noise (Duct 2L).

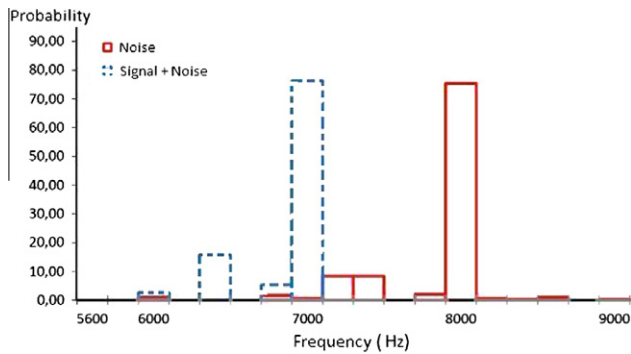


Fig. 9. Column diagrams for signal and signal + noise (Duct 4R).

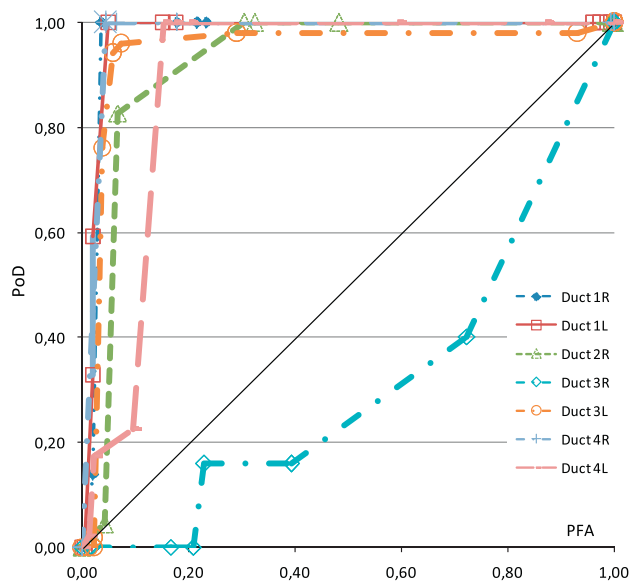


Fig. 10. ROC curves for all ducts in the test sample.

decrease is about 10% from ordinary to highly reinforced concrete sections for the empty ducts 2R, 4L 4R, and reaches 25% for the empty duct with high thickness (3R). This benefit is of course dependent on the protocol, and other studies will be devoted to the protocol optimization depending of the concrete condition around the duct and the duct thickness.

4.4. Assessment of detection threshold

For all the cases (1R,2R,4R,4L) with low δ_{NDT} value, the obtained detection threshold is 7.1 kHz, which is computed using

Table 3

Values of δ_{NDT} (unitless) for each duct in ordinary and highly reinforced concrete and relative deviation (%).

Ducts	Ordinary concrete	Highly reinforced concrete	Relative deviation (%)
Duct 1L	0.18	0.085	-9.5
Duct 1R	0.125	0.025	-10
Duct 2R	0.141	0.025	-11.5
Duct 3L	0.16	0.065	-9.5
Duct 3R	0.867	0.593	-27.5
Duct 4L	0.132	0.025	-10.5
Duct 4R	0.134	0.025	-11

Table 4

Values of PoD and PFA for a detection threshold of 7100 kHz (ducts 1R, 2R, 4R, 4L).

Ducts	PoD	PFA
Duct 1R	1	0.02
Duct 2R	1	0.3
Duct 4L	1	0.04
Duct 4R	1	0.15

Table 5

Values of PoD and PFA for a detection threshold of 7100 kHz (ducts 1L, 2L, 3L, 3R).

Ducts	PoD	PFA
Duct 1L	0.59	0.02
Duct 2L	0.22	0.13
Duct 3L	0.94	0.06
Duct 3R	0	0.21

the coordinates of the closer point to the BPP and Eqs. (4), (5) for each ROC curve. Related values of PoD and PFA are given in Table 4 for the ordinary concrete section. PFA values vary, but are always less than 0.3.

For this detection threshold of 7.1 kHz, Table 5 gives the values of PoD and PFA obtained for the 3 other duct cases (3R, 1L, 3L) and for the 2L case with filled duct. The highest probability of detection, a value of 0.94, is obtained for the duct that is fully filled with epoxy. This case has been included inside the wall to illustrate that impact-echo signals are dependent on the local stiffness. Similarly to the results obtained on duct 3R, it advocates for the use of 2-D measurement grids that makes possible comparison above and outside the duct. When analyzing results of case 2L, where the duct was normally filled with grout, it is shown that, for a detection threshold of 7.1 kHz, the probability of detection is the worst (except the case 3R) and reaches a value of only 0.22.

5. Discussion

The methodology presented in this paper is based on analysis of impact echo signals. This methodology is shown to be very efficient if a calibration is made first, i.e. the underlying state is known. But this calibration is not mandatory if the exact position of ducts within the structure is known; thus the 'noise' can be characterized and the great amount of data collected by the robot enables ROC curves to be plotted. The PFA provides a rational tool, through the ROC curve, for the assessment of the best detection threshold in terms of distance to the best performance point.

Note that we specifically avoid the 'fully filled duct with concrete' case (2L) as a reference, i.e. 'case without defect'. In fact the response i.e. peak frequency of the empty duct depends on the type of concrete. Such a reference value depends on the stiffness of the concrete around the duct and no reference value can be defined in the general case of on site measurements. It would

be poor practice to use a reference case that changes along the structure when the concrete changes itself.

6. Conclusions

This paper reports the results from 994 contactless impact-echo tests carried out on a reinforced concrete wall containing simulated tendon ducts. The aim of this effort is to detect voids in the grout fill within the ducts, and to balance the need of identification of defects with the necessity to increase the probability of detection in case of an 'empty' duct. We confirm the expected reduction of impact-echo peak frequency when tests are carried out nearby a void defect, and further we show this to be caused by an effective reduction of through-thickness section stiffness. The data are analyzed statistically where the probability of detection and the probability of false alarm for seven different duct conditions are considered. The α - δ method is shown to be a rational approach to characterize detection capability of the impact-echo technique for these test cases; cases where the duct is filled and cases with a void are distinguished. Furthermore, this approach allows the user to calibrate the detection threshold to be used on site in order to minimize the probability of false alarm and maximize the probability of detection, and to quantify the detection capability and rank protocols. This last point will be investigated further in future work where variation of experimental characteristics, such as the impact force and diameter of the ball, and consideration of new signal information, such as signal bandwidth, will be studied.

Acknowledgements

We would like to thank the French National Agency for Research (ANR) and Electricité De France (EDF) for funding this research within the project ACTENA. We would like to acknowledge the significant help of Louis-Marie Cottineau, Fabrice Blaineau, Alain Grosseau (Ifsttar, MACS) and Michel Valade (LRPC, Lyon) for the design and realization of the robot. The building of the wall was performed under the supervision of Bernard Guieysse (Ifsttar, IM) and the tendon duct preparation was carried out by Jean-Francois David (Ifsttar, SOA). MSc students Thibault Delacourt, Daniel Lerat and Guillaume Levillain are also thanked.

References

- [1] Faber MH. RBI: an introduction. *Struct Eng Int* 2002;3:187–94.
- [2] Breyse D, Elachachi SM, Sheils E, Schoefs F, O'Connor A. Life cycle cost analysis of ageing structural components based on nondestructive condition assessment. *Aust J Struct Eng* 2009;9(1):55–66.
- [3] Sheils E, O'Connor A, Breyse D, Schoefs F, Yotte S. Development of a two-stage inspection process for the assessment of deteriorating bridge structures. *Rel Eng System Safety* 2010;95(3):182–94. doi:10.1016/j.res.2009.09.00.
- [4] Sheils E, O'Connor A, Schoefs F, Breyse D. Investigation of the effect of the quality of inspection techniques on the optimal inspection interval for structures", structure and infrastructure engineering: maintenance, management, Life-Cycle Design and performance (NSIE), special issue "monitoring, modeling and assessment of structural deterioration in marine environments", first published on 10 August 2010 iFirst, vol. 8(6). Taylor & Francis, June 1st 2011, doi: 10.1080/15732479.2010.5053772.
- [5] Schoefs F. Risk analysis of structures in presence of stochastic fields of deterioration: coupling of inspection and structural reliability. *Aus J Struct Eng* 2009;9(1) [Special Issue "Disaster & Hazard Mitigation"].
- [6] Rouhan A, Schoefs F. Probabilistic modelling of inspections results for offshore structures. *Struct Safety* 2003;25:379–99.
- [7] Pakrashi V, Schoefs F, Memet JB, O'Connor A. ROC dependent event isolation method for image processing based assessment of corroded harbour structures. *Struct Inf Eng: Maint Manage Life-Cycle Design Perform* 2010;6(3):365–78.
- [8] Schoefs F, Clément A, Nouy A. Assessment of spatially dependent ROC curves for inspection of random fields of defects. *Struct Safety* 2009;31(5):409–19, doi:dx.doi.org/10.1016/j.strusafe.2009.01.004 [Published on line March 26th 2009].
- [9] Schoefs F, Clément A. Multiple inspection modeling for decision making and management of jacket off-shore platforms: effect of false alarms. In *First international forum on engineering decision making (IFED'04)*, December 5–9 2004. Stoos, Switzerland.
- [10] Schoefs F, Clément A, Boéro J, Capra B. The $\alpha\delta$ method for modeling expert judgment and combination of NDT tools in RBI context: application to marine structures. In: *Structure and infrastructure engineering: maintenance, management, Life-Cycle Design and performance (NSIE)*, Special issue "monitoring, modeling and assessment of structural deterioration in marine environments", First published online 16 sept. 2010, p. 1744–8980, doi:10.1080/15732479.2010.505374.
- [11] Barnouin B, Lemoine L, Dover WD, Rudlin JR, Fabbri S, Rebourget G, et al. Underwater inspection reliability trials for offshore structures. In: *Proceedings of the 12th international conference on offshore mechanics and arctic engineering* 1993;2:883–90.
- [12] Rudlin JR. Reliability of inspection for fatigue cracks in offshore structures. Savoy Place, London WC2R OBL, UK: Institution of Electrical Engineers; 1996. p. 6/1–3.
- [13] Baroth J, Schoefs F, Breyse D. (coord). *Construction reliability*. ISTE Ltd -Wiley; 2011. 368 p.
- [14] Sansalone MJ, Streett WB. *Impact echo: non-destructive evaluation of concrete and masonry*. Bullbrier Press; 1997.
- [15] Gibson A, Popovics JS. Lamb wave basis for impact-echo method analysis. *ASCE J Eng Mech* 2005;131(4):438–43.
- [16] Prada C, Clorennec D, Royer D. Power law decay of zero-group velocity lamb modes. *Wave Motion* 2008;45(6):723–8.
- [17] Abraham O, Côte Ph. Impact-echo thickness frequency profile for the detection of voids in tendon duct. *ACI Struct J* 2002;99(3):239–47.
- [18] Algernon D, Grafe B, Mielentz F, Kolher B, Schubert F. Imaging of elastic wave propagation in concrete using scanning techniques: application for impact-echo and ultrasonic echo methods. *J Nondestruct Eval* 2008;27(1-3):83–97.